Supplemental material

Edzuka and Goshima, https://doi.org/10.1083/jcb.201807077

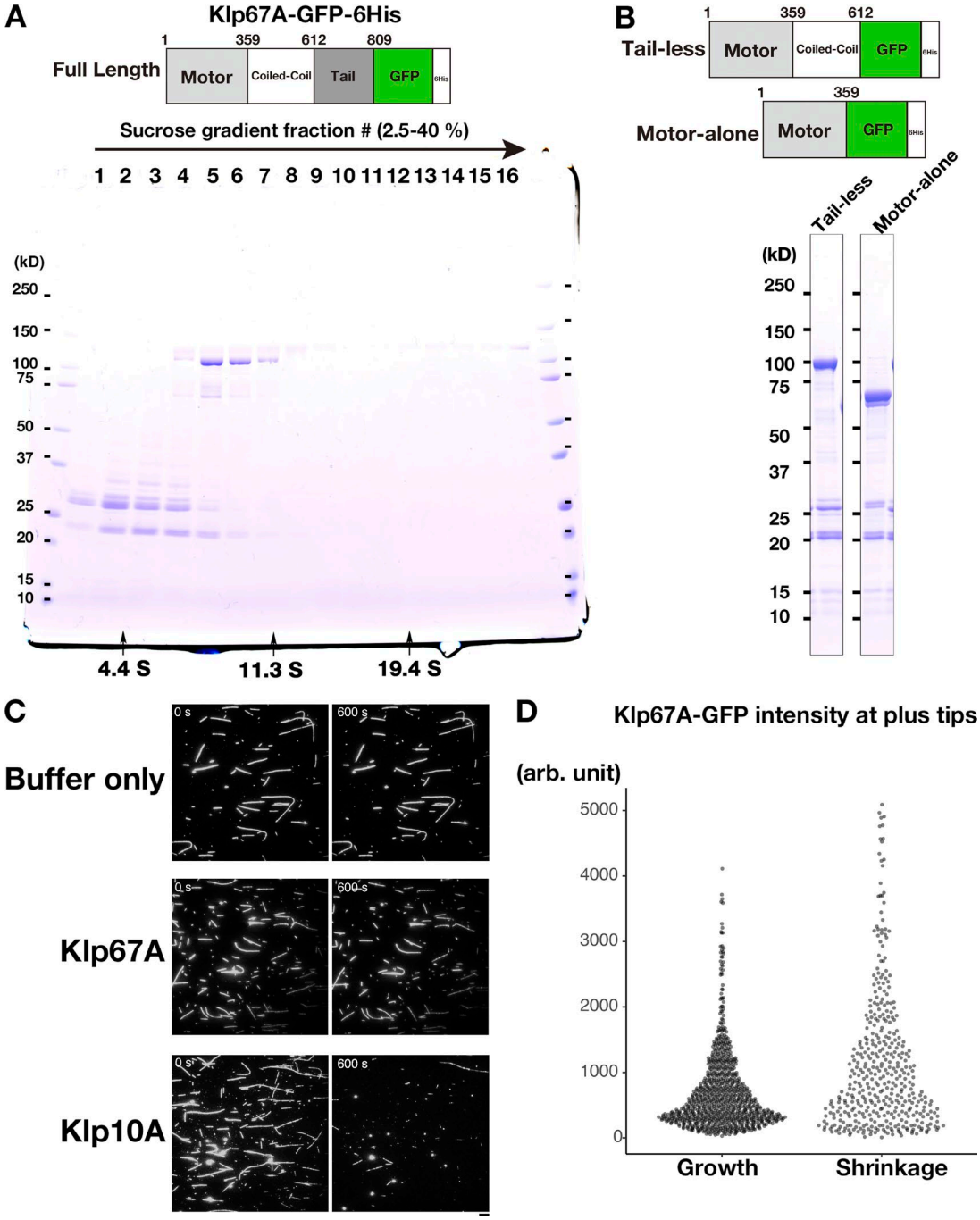

Figure S1. **Purification of kinesin-8^{Klp67A}-GFP. (A)** Coomassie staining of full-length kinesin-8^{Klp67A} tagged with GFP and 6× His after sucrose gradient centrifugation. BSA, catalase, and thyroglobulin were used as the markers (indicated by arrows). Fraction 6 was used for activity measurement. **(B)** Coomassie staining of purified, truncated kinesin-8^{Klp67A} tagged with GFP and 6× His. **(C)** Kinesin-8^{Klp67A} (10 nM) cannot depolymerize GMPCPP-stabilized MTs. MTs stabilized with GMPCPP were mixed with full-length kinesin-8^{Klp67A} (10 nM) and, as a positive control, MT depolymerase kinesin-13^{Klp10A} (10 nM). Bar, 5 µm. **(D)** Kinesin-8^{Klp67A}-GFP intensities at the plus ends of growing and shrinking MTs (n = 891 and 409). The intensity was, on average, slightly higher on shrinking MTs ($P < 0.001$; Brunner-Munzel test).

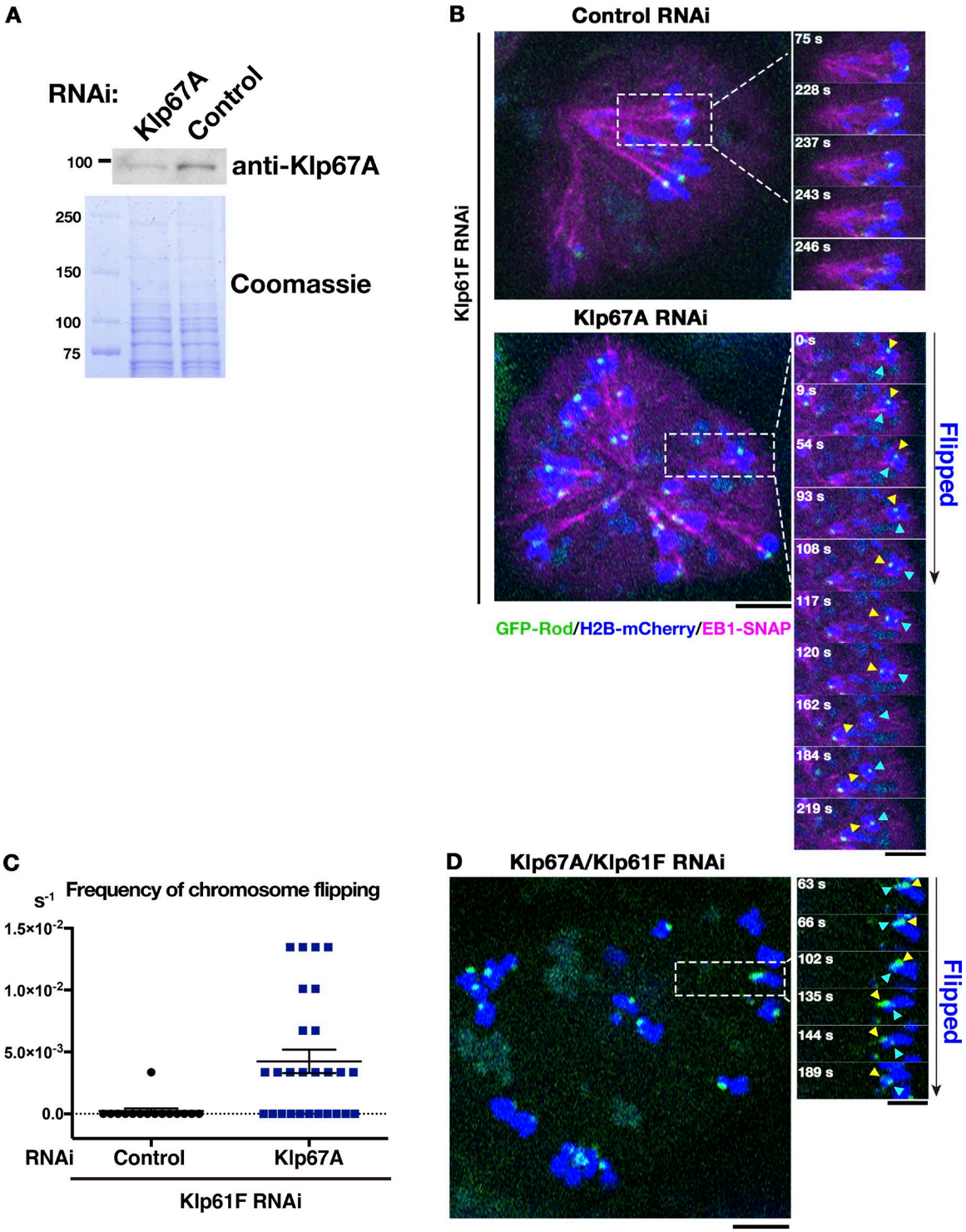

Figure S2. **Kinesin-8^{Klp67A} RNAi causes MT attachment instability. (A)** Immunoblotting confirmed 80% reduction of kinesin-8^{Klp67A} protein after RNAi (GFP-CLASP$^{Mast/Orbit}$ expressing line was used). **(B–D)** MT attachment instability was not an artifact of SiR-tubulin staining, as the phenotype was reproduced without SiR-tubulin staining. In B, MTs were visualized by expressing fluorescently labeled EB1, whereas MTs were not labeled in D. **(C)** Chromosome flipping frequency was quantified (per cell, per second; ± SEM). 15 cells and 27 cells were analyzed (control and Klp67A RNAi). Bars, 5 µm.

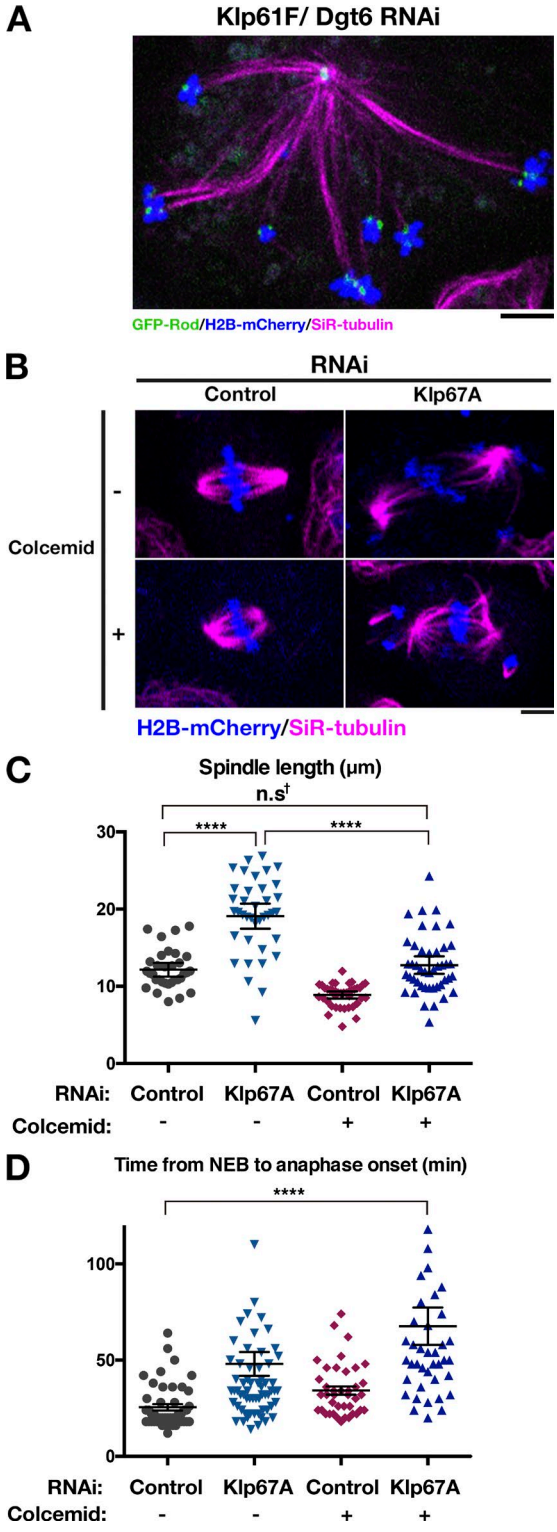

Figure S3. **Artificial MT shortening cannot rescue chromosome misalignment induced by kinesin-8^{Klp67A} depletion. (A)** Elongated monopolar spindle after double RNAi knockdown of augmin^{Dgt6} and kinesin-5^{Klp61F}. GFP-Rod signals indicated the presence of both monotelic and syntelic chromosomes. See Video 4 for chromosome/kinetochore dynamics. **(B–D)** Force shortening of the spindle by colcemid treatment (60 ng/ml) in kinesin-8^{Klp67A} RNAi-treated cells did not recover chromosome misalignment (B) and mitotic progression (D), despite that the spindle was shortened to the control level (C). Spindle length was measured at 16 min after nuclear envelope breakdown. Marked with † is the comparison between control RNAi and Klp67A RNAi + colcemid: mean difference = 0.59; 95% confidence interval on the difference = [−1.28, 2.46]. **** indicates significant ($P < 0.001$) difference by Games-Howell test. n = 33, 38, 45, and 40 (C; from left to right) and 46, 66, 40, and 41 (D; from left to right). Error bars indicate SEM. Experiments were performed twice, and the data from one experiment is presented. Two outliers obtained in kinesin-8^{Klp67A} RNAi-treated cells in D are not described in the graph, but were taken into account during mean and SEM calculations. Bars, 5 μm.

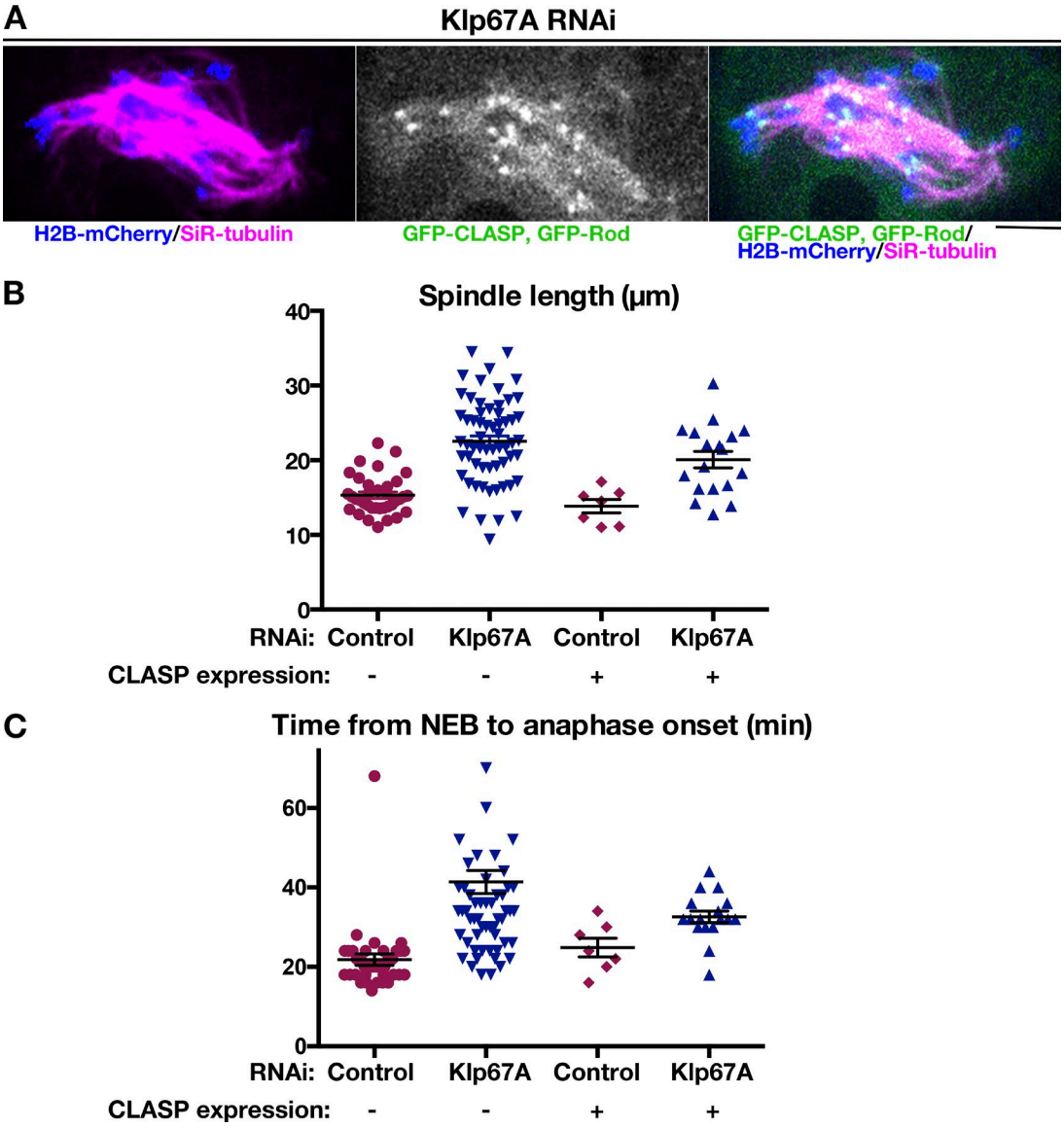

Figure S4. **CLASP$^{Mast/Orbit}$ overexpression cannot rescue chromosome misalignment induced by kinesin-8^{Klp67A} depletion. (A)** A typical mitotic cell expressing GFP-CLASP$^{Mast/Orbit}$ following kinesin-8^{Klp67A} RNAi. Chromosomes were severely misaligned in the spindle. **(B and C)** Metaphase spindle length and mitotic delay were also not rescued by CLASP$^{Mast/Orbit}$ overexpression (error bars represent SEM).

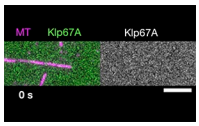

Video 1. **Processive motility and plus end accumulation of kinesin-8^{Klp67A}.** Kinesin-8^{Klp67A}-GFP was imaged every 1 s with TIRF microscopy. We first illuminated the imaging field for ∼3 min with high laser power to bleach most, if not all, kinesin-8^{Klp67A}-GFP at the MT end and then restarted time-lapse imaging with a normal laser power. Bar, 5 µm.

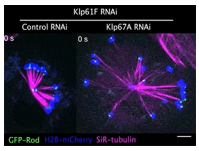

Video 2. **MT attachment stability in the monopolar spindle in the presence or absence of kinesin-8^{Klp67A}.** GFP-Rod (green), H2B-mCherry (blue), and SiR-tubulin (magenta) images were acquired every 3 s with spinning-disc confocal microscopy in kinesin-5^{Klp61F} single or kinesin-8^{Klp67A}/kinesin-5^{Klp61F} double RNAi-treated cells. Bar, 5 µm.

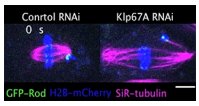

Video 3. **MT attachment stability in the bipolar spindle in the presence or absence of kinesin-8^{Klp67A}.** GFP-Rod (green), H2B-mCherry (blue), and SiR-tubulin (magenta) images were acquired every 3 s with spinning-disc confocal microscopy in kinesin-8^{Klp67A} or control RNAi-treated cells. Bar, 5 µm.

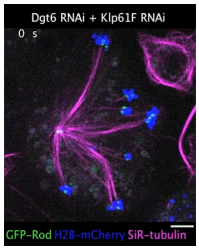

Video 4. **MT attachment stability in the absence of augmin^{Dgt6}.** GFP-Rod (green), H2B-mCherry (blue), and SiR-tubulin (magenta) images were acquired every 3 s with spinning-disc confocal microscopy in augmin^{Dgt6}/kinesin-5^{Klp61F} RNAi-treated cells. Bar, 5 µm.

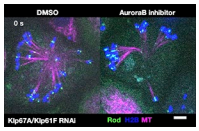

Video 5. **Stable syntelic attachment in the monopolar spindle after Aurora B inhibition in the absence of kinesin-8^{Klp67A}.** GFP-Rod (green), H2B-mCherry (blue), and SiR-tubulin (magenta) images were acquired every 3 s with spinning-disc confocal microscopy in augmin^{Dgt6}/kinesin-5^{Klp61F} RNAi-treated cells. 20 µM Binucleine-2 (*Drosophila* Aurora B inhibitor) or control DMSO was added at time 0. Bar, 5 µm.

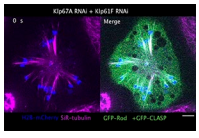

Video 6. **CLASP$^{Mast/Orbit}$ overexpression rescued MT attachment stability in the absence of kinesin-8^{Klp67A}.** GFP-Rod (green), GFP-CLASP$^{Mast/Orbit}$ (green), H2B-mCherry (blue), and SiR-tubulin (magenta) images were acquired every 3 s with spinning-disc confocal microscopy in kinesin-8^{Klp67A}/kinesin-5^{Klp61F} double RNAi-treated cells expressing GFP-CLASP$^{Mast/Orbit}$. Bar, 5 µm.

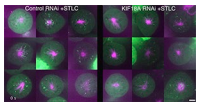

Video 7. **GFP-Mad2 dynamics in the monopolar spindle after KIF18A RNAi in HeLa cells.** GFP-Mad2 (green) and SiR-tubulin (magenta) images were acquired every 4 s with spinning-disc confocal microscopy in kinesin-8^{KIF18A} and control RNAi-treated cells that were treated with STLC, an inhibitor of kinesin-5^{Eg5}. Nine randomly selected cells are displayed for each sample. Areas devoid of fluorescence represent chromosomes. Neither of the authors could identify any phenotype associated with kinesin-8^{KIF18A} depletion. Bar, 5 µm.

Table S1. **Plasmids used in this study**

Name	Insert	Vector	Note
pED128	Klp67A[full-length]-GFP-6His	pET23	
pED182	Klp67A[1–612aa]-GFP-6His	pET23	
pED183	Klp67A[1–359aa]-GFP-6His	pET23	
pGG952	6His-Klp10A	pDEST17	Moriwaki and Goshima (2016)
pED158	sfGFP-Rod	pAc	
pGFP-CLASP	GFP-Mast/Orbit	pMT	Goshima et al. (2007)
pGG482	H2B-mCherry	pAc	
pED309	EB1-SNAP	pAc	
pCoHygromycin	HygR	Copia	

References

Goshima, G., R. Wollman, S.S. Goodwin, N. Zhang, J.M. Scholey, R.D. Vale, and N. Stuurman. 2007. Genes required for mitotic spindle assembly in Drosophila S2 cells. *Science.* 316:417–421. https://doi.org/10.1126/science.1141314

Moriwaki, T., and G. Goshima. 2016. Five factors can reconstitute all three phases of microtubule polymerization dynamics. *J. Cell Biol.* 215:357–368. https://doi.org/10.1083/jcb.201604118